Chemical potential of a test hard sphere of variable size in hard-sphere fluid mixtures

David M. Heyes[1,a] and Andrés Santos[2,b]
[1]*Department of Physics, Royal Holloway, University of London, Egham, Surrey TW20 0EX, United Kingdom*
[2]*Departamento de Física and Instituto de Computación Científica Avanzada (ICCAEx), Universidad de Extremadura, E-06071 Badajoz, Spain*

(Received 28 April 2018; accepted 16 May 2018; published online 6 June 2018)

A detailed comparison between the Boublík–Mansoori–Carnahan–Starling–Leland (BMCSL) equation of state of hard-sphere mixtures is made with Molecular Dynamics (MD) simulations of the same compositions. The Labík and Smith simulation technique [S. Labík and W. R. Smith, Mol. Simul. **12**, 23–31 (1994)] was used to implement the Widom particle insertion method to calculate the excess chemical potential, $\beta\mu_0^{\rm ex}$, of a test particle of variable diameter, σ_0, immersed in a hard-sphere fluid mixture with different compositions and values of the packing fraction, η. Use is made of the fact that the only polynomial representation of $\beta\mu_0^{\rm ex}$ which is consistent with the limits $\sigma_0 \to 0$ and $\sigma_0 \to \infty$ has to be of the cubic form, i.e., $c_0(\eta) + \bar{c}_1(\eta)\sigma_0/M_1 + \bar{c}_2(\eta)(\sigma_0/M_1)^2 + \bar{c}_3(\eta)(\sigma_0/M_1)^3$, where M_1 is the first moment of the distribution. The first two coefficients, $c_0(\eta)$ and $\bar{c}_1(\eta)$, are known analytically, while $\bar{c}_2(\eta)$ and $\bar{c}_3(\eta)$ were obtained by fitting the MD data to this expression. This in turn provides a method to determine the excess free energy per particle, $\beta a^{\rm ex}$, in terms of $\bar{c}_2$, $\bar{c}_3$, and the compressibility factor, Z. Very good agreement between the BMCSL formulas and the MD data is found for $\beta\mu_0^{\rm ex}$, Z, and $\beta a^{\rm ex}$ for binary mixtures and continuous particle size distributions with the top-hat analytic form. However, the BMCSL theory typically slightly underestimates the simulation values, especially for Z, differences which the Boublík–Carnahan–Starling–Kolafa formulas and an interpolation between two Percus–Yevick routes capture well in different ranges of the system parameter space. *Published by AIP Publishing.* https://doi.org/10.1063/1.5037856

I. INTRODUCTION

Particulate mixtures are widely encountered in the real world, in the form of powders and liquid mixtures. For many years, there has been an active interest in studying such "granular" mixtures in numerous fields, such as in chemistry, geology, pharmaceutical science, food technology, and in various aspects of chemical engineering processing and civil engineering. They are intrinsically difficult to understand and control. The hard sphere (HS) particle has proven a useful reference fluid for single component liquids, and it makes logical sense to use the same type of model particle to act as a starting point to represent and understand the physical behavior of such multicomponent systems. Mixtures of HSs of different size distributions (discrete or continuous) can similarly be used to model, for instance, nanocolloidal liquids and granular materials. Mixtures are more problematic than single component liquids to deal with theoretically as there are more parameters to be accounted for in any theoretical treatment. In the binary mixture HS case, these are the total packing fraction, η, the diameters of the two spheres, σ_1 and σ_2, their mole fractions, x_1 and $x_2 = 1 - x_1$, and for dynamical properties, their masses. Therefore, the statistical mechanical theory of the equation of state (EoS) and derived properties poses a much greater challenge than for the single component. One of the most widely used approximate analytic EoSs for mixtures is that of Boublík–Mansoori–Carnahan–Starling–Leland (BMCSL).[1,2] This has been found to be an accurate representation of the available simulation data.[3–9] However, a comprehensive exploration of its performance over the possible ranges of this parameter space is yet to be carried out. This is particularly for the chemical potential of a test particle in the regions of this parameter space which would better assess the overall accuracy of the BMCSL EoS.

Here, a systematic exploration of the accuracy of the BMCSL EoS over a wide parameter range is carried out using new computer simulation data of a binary mixture of HSs and a closely related so-called top-hat (TH) continuous diameter distribution between lower and higher values, σ_2 and σ_1, respectively. The chemical potential of a test particle of varying diameter, σ_0, inserted into the mixture is calculated using the Widom particle insertion method.[10]

The method employed here was first used for HS systems by Monte Carlo (MC) simulations for the single component case by Labík and Smith[11] and later applied to a binary mixture of HSs by Barošová *et al.*[4] The technique measures the probability of the successful insertion of a test particle of arbitrary diameter σ_0. These measurements are extrapolated with a suitable polynomial in powers of σ_0 to give the chemical potential of tracer particles larger than can be

[a]Electronic mail: david.heyes@rhul.ac.uk
[b]Electronic mail: andres@unex.es. URL: http://www.unex.es/eweb/fisteor/andres/.

practically inserted in the simulations. We first applied this method in Molecular Dynamics (MD) simulations to the single component fluid using a third-degree polynomial.[12] In the Appendix of Ref. 12, we proved that a polynomial consistent with the limits $\sigma_0 \to 0$ and $\sigma_0 \to \infty$ must necessarily have a cubic form, regardless of the number of components. To be consistent with this fact, we assume here a third-degree polynomial, even in the multicomponent case, rather than a fourth- or fifth-degree polynomial which was used in Ref. 4. The highest two coefficients so obtained by fitting the simulation test particle chemical potential data to the polynomial are used here to compute the free energy per particle of the mixture, which is a novel outcome of this numerical study. Recently, Baranau and Tallarek[13] employed an alternative solution which consisted of measuring the so-called pore-size distribution, fitting it to a Gaussian, and then performing analytically an integral to determine the chemical potential. Other methods use a particle swap scheme[14] or well-tempered metadynamics.[15,16] We note in passing that alternative analytic forms for the EoS to the BMCSL equation have been proposed and compared against simulation data.[8,17–22]

The remainder of this work is organized as follows. Expressions are reviewed in Sec. II and the use of a cubic polynomial as a trial function for $\beta\mu_0^{\text{ex}}$ is justified. The computer simulation method is briefly described in Sec. III. The results are presented and compared with theoretical predictions in Sec. IV, and some conclusions are given in Sec. V.

II. THEORY

A. Equation of state of multicomponent hard-sphere fluids

Consider a three-dimensional fluid mixture of additive HSs with an arbitrary number of components, in which for each species j, there are N_j spheres of diameter σ_j. The total number of particles is $N = \sum_j N_j$ and the nth moment of the size distribution is

$$M_n = \sum_j x_j \sigma_j^n, \tag{2.1}$$

where $x_j = N_j/N$ is the mole fraction of species j (with $\sum_j x_j = 1$). The total packing or volume fraction of the HS mixture is exactly defined as

$$\eta = \frac{\pi}{6}\frac{N}{V} M_3, \tag{2.2}$$

where V is the volume of the system.

The compressibility factor of the mixture is denoted by $Z(\eta, \{x_j\}) \equiv \beta pV/N$, where p is the pressure, $\beta = 1/k_B T$, k_B is Boltzmann's constant, and T is the absolute temperature. The exact form of Z as a function of these parameters is not known, and several approximations have been proposed.[8,23]

The exact solution[24–26] of the Percus–Yevick (PY) integral equation[27] leads to explicit expressions for Z by different thermodynamic routes. Specifically, the virial (PY-v), compressibility (PY-c), and chemical-potential (PY-μ) routes in the PY approximation have a common structure,[24–26,28–30]

$$\begin{aligned} Z(\eta, \{x_j\}) &= Z_0(\eta) + Z_1(\eta)\frac{M_1 M_2}{M_3} + Z_2(\eta)\frac{M_2^3}{M_3^2} \\ &= Z_0(\eta) + Z_1(\eta)\lambda + Z_2(\eta)\frac{\lambda^3}{\gamma}, \end{aligned} \tag{2.3}$$

where

$$Z_0(\eta) = \frac{1}{1-\eta}, \quad Z_1(\eta) = \frac{3\eta}{(1-\eta)^2}, \tag{2.4}$$

$$\lambda(\{x_j\}) \equiv \frac{M_1 M_2}{M_3}, \quad \gamma(\{x_j\}) \equiv \frac{M_1^3}{M_3}. \tag{2.5}$$

Of course, $\lambda = \gamma = 1$ is the single component case. In general, as proved in Ref. 31, one has $\lambda^2 \le \gamma \le \lambda \le 1$, regardless of the number of components. The functions (2.4) are the same in all the PY EoSs, while the function $Z_2(\eta)$ depends on the route and is displayed in the second column of Table I. It must be noted that the PY-c EoS is equivalent to the Scaled Particle Theory (SPT) approximation,[32–36] and this is why it is labeled as "PY-c (SPT)" in Table I.

Equation (2.3) provides a method to extend any single component HS compressibility factor, $Z_s(\eta)$, to multicomponent fluids simply by choosing

$$Z_2(\eta) = Z_s(\eta) - \frac{1+2\eta}{(1-\eta)^2}, \tag{2.6}$$

although other alternative methods are possible.[8,37–40] In particular, if $Z_s(\eta)$ is chosen to be the Carnahan–Starling[41] or the Carnahan–Starling–Kolafa[42] EoSs, application of Eqs. (2.3) and (2.6) yields the BMCSL or Boublík–Carnahan–Starling–Kolafa (BCSK)[43] extensions, respectively. The corresponding expressions for $Z_2(\eta)$ are also presented in Table I.

As is well known, the BMCSL compressibility factor is an interpolation between the PY-v and PY-c prescriptions, namely,

$$Z^{\text{BMCSL}}(\eta) = \frac{1}{3}Z^{\text{PY-v}}(\eta) + \frac{2}{3}Z^{\text{PY-c}}(\eta). \tag{2.7}$$

Given that the PY-μ route is slightly more accurate than the PY-v one,[29,30] an alternative interpolation formula is

$$Z^{\text{PY-}\mu\text{c}}(\eta) = \alpha Z^{\text{PY-}\mu}(\eta) + (1-\alpha)Z^{\text{PY-c}}(\eta), \tag{2.8}$$

with $\alpha \simeq 0.37$.

B. Free energy of multicomponent hard-sphere fluids

The thermodynamic relation between the excess free energy per particle, $a^{\text{ex}}(\eta, \{x_j\})$, and the compressibility factor, $Z(\eta, \{x_j\})$, is

$$\beta a^{\text{ex}}(\eta, \{x_j\}) = \int_0^1 dt \frac{Z(\eta t, \{x_j\}) - 1}{t}. \tag{2.9}$$

Therefore, if Z has the form in Eq. (2.3), then

$$\beta a^{\text{ex}}(\eta, \{x_j\}) = c_0(\eta) + c_1(\eta)\lambda + a_2(\eta)\frac{\lambda^3}{\gamma}, \tag{2.10}$$

where

$$c_0(\eta) = -\ln(1-\eta), \quad c_1(\eta) = \frac{3\eta}{1-\eta}, \tag{2.11a}$$

TABLE I. Expressions for $Z_2(\eta)$, $a_2(\eta)$, $c_2(\eta)$, and $c_3(\eta)$, according to several approximations.

Approx.	$Z_2(\eta)$	$a_2(\eta)$	$c_2(\eta)$	$c_3(\eta)$
PY-v	$\frac{3\eta^2}{(1-\eta)^2}$	$3\ln(1-\eta)+\frac{3\eta}{1-\eta}$	$9\ln(1-\eta)+12\frac{\eta}{1-\eta}$	$-6\ln(1-\eta)-\eta\frac{5-11\eta}{(1-\eta)^2}$
PY-c (SPT)	$\frac{3\eta^2}{(1-\eta)^3}$	$\frac{3\eta^2}{2(1-\eta)^2}$	$3\eta\frac{2+\eta}{2(1-\eta)^2}$	$\eta\frac{1+\eta+\eta^2}{(1-\eta)^3}$
PY-μ	$-\frac{9\ln(1-\eta)}{\eta}-9\frac{1-\frac{3}{2}\eta}{(1-\eta)^2}$	$\frac{9\ln(1-\eta)}{\eta}+9\frac{1-\frac{1}{2}\eta}{1-\eta}$	$27\frac{\ln(1-\eta)}{\eta}+3\frac{18-7\eta}{2(1-\eta)}$	$-27\frac{\ln(1-\eta)}{\eta}-\frac{54-83\eta+14\eta^2}{2(1-\eta)^2}$
BMCSL	$\frac{\eta^2(3-\eta)}{(1-\eta)^3}$	$\ln(1-\eta)+\frac{\eta}{(1-\eta)^2}$	$3\ln(1-\eta)+3\eta\frac{2-\eta}{(1-\eta)^2}$	$-2\ln(1-\eta)-\eta\frac{1-6\eta+3\eta^2}{(1-\eta)^3}$
BCSK	$\frac{\eta^2[3-\frac{2}{3}\eta(1+\eta)]}{(1-\eta)^3}$	$\frac{8}{3}\ln(1-\eta)$ $+\eta\frac{16-15\eta+4\eta^2}{6(1-\eta)^2}$	$8\ln(1-\eta)+\eta\frac{22-21\eta+4\eta^2}{2(1-\eta)^2}$	$-\frac{16}{3}\ln(1-\eta)$ $-\eta\frac{13-43\eta+27\eta^2-2\eta^3}{3(1-\eta)^3}$

$$a_2(\eta)=\int_0^1 dt\,\frac{Z_2(\eta t)}{t}. \tag{2.11b}$$

The expressions for $a_2(\eta)$ corresponding to several approximations are also presented in Table I.

C. Chemical potential of a test sphere

Now, we want to obtain from Eq. (2.10) the theoretical excess chemical potential of a test particle (of diameter σ_0) immersed in a HS mixture. To that end, note first that the excess chemical potential of a generic species i is thermodynamically defined as

$$\beta\mu_i^{\text{ex}}=\left(\frac{\partial N\beta a^{\text{ex}}}{\partial N_i}\right)_{V,N_{j\neq i}}. \tag{2.12}$$

Next, $\beta\mu_0^{\text{ex}}$ is obtained from $\beta\mu_i^{\text{ex}}$ by the replacement $\sigma_i\to\sigma_0$ while keeping the composition of the mixture fixed. From Eq. (2.10), one finally obtains[12]

$$\beta\mu_0^{\text{ex}}(\sigma_0)=c_0+\bar{c}_1\frac{\sigma_0}{M_1}+\bar{c}_2\left(\frac{\sigma_0}{M_1}\right)^2+\bar{c}_3\left(\frac{\sigma_0}{M_1}\right)^3, \tag{2.13}$$

where

$$\bar{c}_1=\lambda\frac{3\eta}{1-\eta}, \tag{2.14a}$$

$$\bar{c}_2=\lambda^2c_2+(\gamma-\lambda^2)\frac{3\eta}{1-\eta}, \tag{2.14b}$$

$$\bar{c}_3=\lambda^3c_3+(\gamma-\lambda^3)\frac{\eta}{1-\eta}+\lambda(\gamma-\lambda^2)\frac{3\eta^2}{(1-\eta)^2}. \tag{2.14c}$$

In Eqs. (2.14b) and (2.14c),

$$c_2(\eta)=\frac{3\eta}{1-\eta}+3a_2(\eta), \tag{2.15a}$$

$$c_3(\eta)=\frac{3\eta}{(1-\eta)^2}+Z_2(\eta)-\frac{2}{3}c_2(\eta). \tag{2.15b}$$

The expressions for $c_2(\eta)$ and $c_3(\eta)$ predicted by several approximations are given in Table I. From Eqs. (2.3), (2.4), (2.14), and (2.15), one can obtain the relationship

$$Z(\eta,\{x_j\})=1+\frac{1}{3}\bar{c}_1+\frac{2}{3}\frac{\lambda\bar{c}_2}{\gamma}+\frac{\bar{c}_3}{\gamma}. \tag{2.16}$$

As mentioned above, the structure of Eq. (2.3), and hence of Eqs. (2.10) and (2.13), is common to several approximate EoSs, such as PY-v, PY-c, PY-μ, BMCSL, BCSK, and, obviously, PY-μc. They all share the coefficients Z_0, Z_1, c_0, and c_1 [see Eqs. (2.4) and (2.11a)] but differ in Z_2, a_2, c_2, and c_3. Only Z_2 is an independent quantity since a_2, c_2, and c_3 are given by Eqs. (2.11b), (2.15a), and (2.15b), respectively.

An analysis, in the case of binary mixtures, of the extremal properties of the combinations of λ and γ appearing in Eqs. (2.3) and (2.14) is presented in the Appendix.

D. Consistency conditions in the limits $\sigma_0\to 0$ and $\sigma_0\to\infty$

As proved in the Appendix of Ref. 12, the exact form of $\beta\mu_0^{\text{ex}}$ in the limit $\sigma_0/M_1\ll 1$ is

$$\beta\mu_0^{\text{ex}}(\sigma_0)=c_0+\bar{c}_1\frac{\sigma_0}{M_1}+\mathcal{O}\left((\sigma_0/M_1)^2\right). \tag{2.17}$$

Therefore, the cubic approximation (2.13) is consistent with the asymptotic behavior (2.17). Moreover, it is noteworthy that if $\beta\mu_0^{\text{ex}}$ is represented by a polynomial in the diameter σ_0, the polynomial must *necessarily* be of the third degree. This is a consequence of the physical requirement that, in the limit of an infinitely large impurity, the condition[39,44,45]

$$\eta Z=M_3\lim_{\sigma_0\to\infty}\frac{\beta\mu_0^{\text{ex}}(\sigma_0)}{\sigma_0^3} \tag{2.18}$$

must be obeyed. Therefore, since $\lim_{\sigma_0\to\infty}\beta\mu_0^{\text{ex}}(\sigma_0)/\sigma_0^3$ can be neither zero nor infinity, the only polynomial approximations consistent with that property are those of the third degree.

In the case of the approximations of the form (2.3), Eq. (2.18) implies

$$Z=\frac{1}{\eta}\frac{\bar{c}_3}{\gamma}. \tag{2.19}$$

However, the PY-v, PY-μ, BMCSL, and BCSK EoSs are not fully consistent with Eq. (2.19). This means that those approximations *qualitatively* agree with the physical requirement (2.18) since $\lim_{\sigma_0\to\infty}\beta\mu_0^{\text{ex}}(\sigma_0)/\sigma_0^3$ = finite but yield

different results for the left- and right-hand sides. The difference between ηZ, as given by Eqs. (2.3) or (2.16), and $\bar{c}_3/\gamma$ can be seen to be

$$\eta Z - \frac{\bar{c}_3}{\gamma} = \frac{\lambda^3}{\gamma}\left[2a_2 - \eta(1-\eta)a_2'\right], \tag{2.20}$$

where $a_2'(\eta) = da_2(\eta)/d\eta$. Thus, a perfect agreement between Eqs. (2.16) and (2.19) is only possible if $a_2' = 2a_2/\eta(1-\eta)$, whose general solution is $a_2 = K\eta^2/(1-\eta)^2$, where K is a constant. The associated one-component third virial coefficient is $b_3 = 7 + 2K$ so that $b_3 = 10$ implies $K = \frac{3}{2}$ and thus one recovers the PY-c (SPT) approximation.

E. Equivalence between different mixtures

According to Eqs. (2.3), (2.10), and (2.14), two mixtures sharing the same values of η, λ, and γ would have common values of Z, βa^{ex}, and $\bar{c}_n$. Having the same values of λ and γ implies having the same values of the reduced moments M_2/M_1^2 and M_3/M_1^3. As a consequence, given any HS mixture (with an arbitrary number of components and arbitrary diameters), it will always be possible to find an "equivalent" binary mixture with the same equilibrium properties. The mole fraction, x_1, of the bigger spheres and the size ratio, $q \equiv \sigma_2/\sigma_1 \leq 1$, for the binary mixture equivalent of a multicomponent system characterized by given values of λ and γ are obtained using the formulas

$$x_1 = \frac{1}{2} - \frac{1 + 2\gamma - 3\lambda}{2\sqrt{1 + 4\gamma - \lambda(6 + 3\lambda - 4\lambda^2/\gamma)}}, \tag{2.21a}$$

$$q = \frac{1 - \lambda - \sqrt{1 + 4\gamma - \lambda(6 + 3\lambda - 4\lambda^2/\gamma)}}{2\left[\lambda(1 + \lambda - \lambda^2/\gamma) - \gamma\right]/(1-\lambda)} - 1. \tag{2.21b}$$

The mapping property discussed above applies as well to a continuous size distribution characterized by a given distribution function $x(\sigma)$, in which case the moments are

$$M_n = \int_0^\infty d\sigma\, x(\sigma)\sigma^n. \tag{2.22}$$

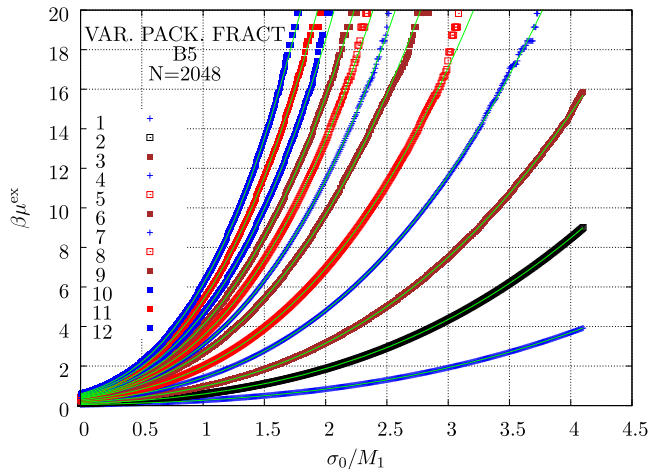

FIG. 1. Plot of the excess chemical potential of a test particle, $\beta\mu_0^{\text{ex}}(\sigma_0)$, for the B5 type of system (see Table II). From right to left, the curves are for η = 0.05, 0.1, 0.15, 0.2, 0.25, 0.3, 0.325, 0.35, 0.375, 0.4, 0.425, and 0.45, respectively, using N = 2048 particles in the MD simulation.

TABLE II. The HS mixture systems analyzed and their tags.

Set	η	x_1	σ_2/σ_1
B1	0.3	0.5	Variable
B2	0.3	Variable	0.5
B3	0.3	Variable	0.3
B4	Variable	0.5	0.5
B5	Variable	0.5	$2-\sqrt{3}$
B6	$(x_1 + 0.1)/2$	Variable	x_1
Set	**η**	**$\sigma_{\min}/\sigma_{\max}$**	
TH1	0.3	Variable	
TH2	Variable	0	

In particular, let us consider a TH continuous size distribution of HSs with diameters between $\sigma_{\min}$ and $\sigma_{\max}$,

$$x_{\text{TH}}(\sigma) = \frac{1}{\sigma_{\max} - \sigma_{\min}} \begin{cases} 1 & \text{if } \sigma_{\min} < \sigma < \sigma_{\max}, \\ 0 & \text{otherwise.} \end{cases} \tag{2.23}$$

The associated values of λ and γ are

$$\lambda_{\text{TH}} = \frac{2}{3}\frac{1 + q_{\text{TH}} + q_{\text{TH}}^2}{1 + q_{\text{TH}}^2}, \quad \gamma_{\text{TH}} = \frac{1}{2}\frac{(1 + q_{\text{TH}})^2}{1 + q_{\text{TH}}^2}, \tag{2.24}$$

where $q_{\text{TH}} = \sigma_{\min}/\sigma_{\max} \leq 1$ is the size ratio. Insertion of Eq. (2.24) into Eqs. (2.21) yields $x_1 = \frac{1}{2}$ and

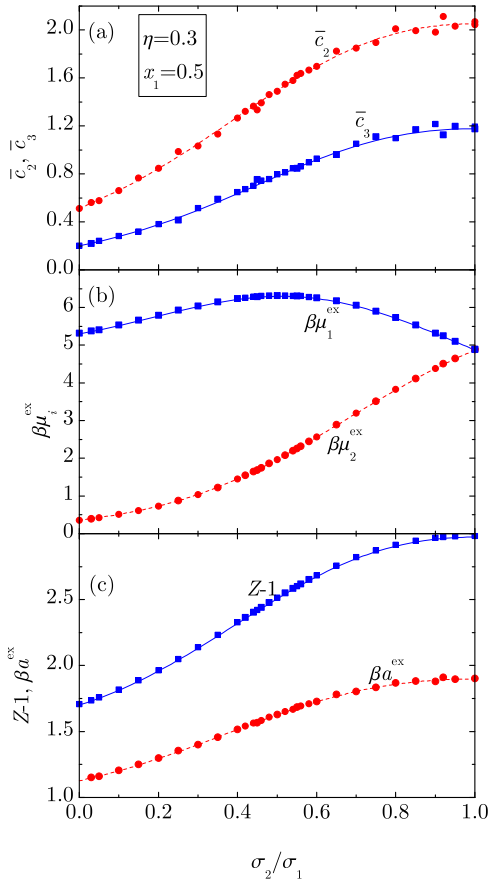

FIG. 2. Plot of (a) $\bar{c}_2$ and $\bar{c}_3$, (b) $\beta\mu_1^{\text{ex}}$ and $\beta\mu_2^{\text{ex}}$, and (c) $Z - 1$ and βa^{ex} versus σ_2/σ_1 for system B1. The symbols are our MD data (N = 2048) and the lines are the BMCSL predictions.

$$q = \frac{q_{\rm TH} + 2 - \sqrt{3}}{1 + (2 - \sqrt{3}) q_{\rm TH}}. \tag{2.25}$$

For instance, if $q_{\rm TH} = 0$, the equivalent binary mixture must have a size ratio $q = 2 - \sqrt{3} \simeq 0.268$. Inversion of Eq. (2.25) gives

$$q_{\rm TH} = \frac{q - (2 - \sqrt{3})}{1 - (2 - \sqrt{3}) q}. \tag{2.26}$$

III. COMPUTER SIMULATIONS

The application of MD and MC computer simulations to HS mixtures goes back to the 1960s.[46,47] The MD simulations carried out in this study employed a generalization of the methodology used in our previous study of single component HSs,[12] using the equations relevant to binary, and hence to multicomponent HS mixtures in general, given by Bannerman and Lue.[48] A test point particle was randomly inserted in the system. If it did not fall within an existing sphere, the distance, r_n, from the point to the center of the nearest sphere, of type k and diameter σ_k, was computed. All the values of $\sigma_0 = 0$ to $\sigma_0 = 2r_n - \sigma_k$ would be allowed insertions which were correspondingly logged. For HSs, the Widom method reduces to a simple bookkeeping procedure as the Boltzmann factor is either 1, if the test sphere (and hence other test particles with diameter less than σ_0) does not overlap with any of the N particles, or is equal to 0, if there is an overlap with any of the other spheres.

The simulations were carried out employing $N = 2048$ particles for typically 2×10^5 collisions per particle. Some additional simulations with $N = 4000$ particles were performed for several of the mixtures to assess the influence of finite-size effects. The pressure and hence Z were obtained by the virial theorem written in terms of the collision parameter. The thermodynamics of the systems is independent of the masses of the spheres, but to facilitate equilibration of the smaller particles, the mass was set to $m_i \propto \sigma_i$ for the binary mixtures and $m(\sigma) \propto \sqrt{\sigma}$ for the TH distributions. The simulations were carried out in the fluid phase diagrams, as these regions are already known for binary[49,50] and polydisperse[51] mixtures.

For each mixture, the excess chemical potential, $\beta\mu_0^{\rm ex}$, was computed by the Widom method as a function of the dimensionless impurity diameter σ_0/M_1. $\mathcal{N}$ attempted particle insertions were made randomly in the system at the same time after every $\mathcal{N}$ collisions. These data were fitted to a cubic polynomial of the form (2.13) using the known *exact* values for c_0 and $\bar{c}_1$ from the expressions in Eqs. (2.11a) and (2.14a), respectively. In fact, c_0 is *universal* in the sense that it is independent of the details of the mixture, apart from the total packing fraction. The parameters, $\bar{c}_2$ and $\bar{c}_3$, were obtained by fitting the simulation values of $\beta\mu_0^{\rm ex}$ to the cubic polynomial in σ_0/M_1. The fitting procedure was applied to values

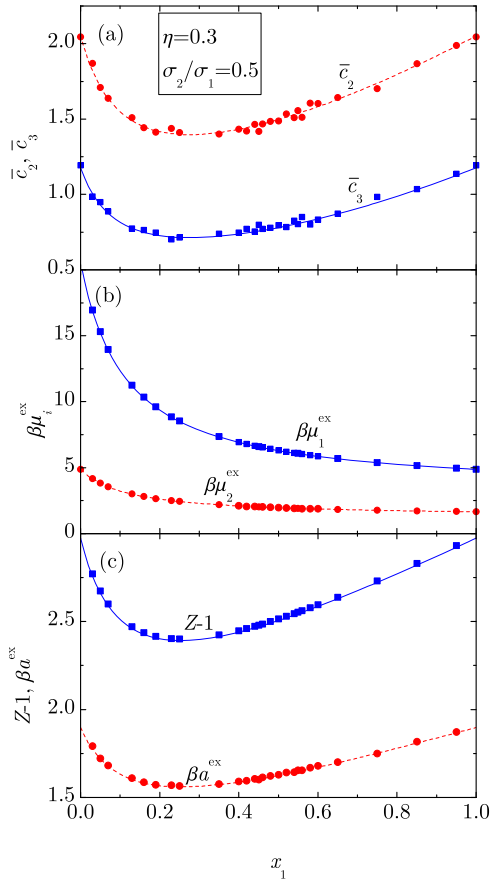

FIG. 3. Plots of (a) $\bar{c}_2$ and $\bar{c}_3$, (b) $\beta\mu_1^{\rm ex}$ and $\beta\mu_2^{\rm ex}$, and (c) $Z - 1$ and $\beta a^{\rm ex}$ versus x_1 for system B2. The symbols are our MD data ($N = 2048$) and the lines are the BMCSL predictions.

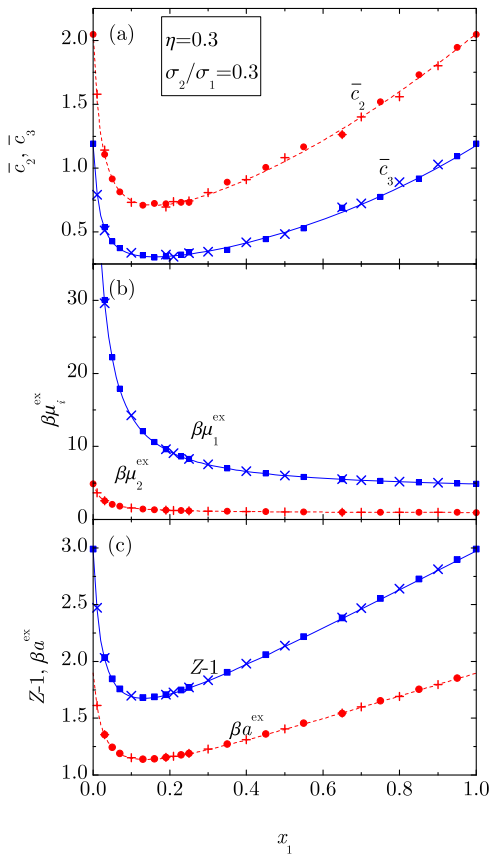

FIG. 4. Plots of (a) $\bar{c}_2$ and $\bar{c}_3$, (b) $\beta\mu_1^{\rm ex}$ and $\beta\mu_2^{\rm ex}$, and (c) $Z - 1$ and $\beta a^{\rm ex}$ versus x_1 for system B3. The symbols are our MD data (filled symbols: $N = 2048$, crosses: $N = 4000$) and the lines are the BMCSL predictions.

$\beta\mu_0^{\rm ex} \leq 16.0$, which corresponds to insertion probabilities larger than $\sim 10^{-7}$. An example of the quality of the fit is shown in Fig. 1.

From the values of Z, $\bar{c}_2$, and $\bar{c}_3$ (and hence $\beta\mu_i^{\rm ex}$) obtained from the simulations, the excess free energy per particle was obtained from the Euler equation of thermodynamics, i.e.,

$$\beta a^{\rm ex} = \sum_i x_i \beta\mu_i^{\rm ex} - Z + 1$$
$$= -\ln(1-\eta) + \lambda\frac{3\eta}{1-\eta} + \frac{\lambda\bar{c}_2}{\gamma} + \frac{\bar{c}_3}{\gamma} - Z + 1, \quad (3.1)$$

where in the last step Eq. (2.13) has been used.

IV. RESULTS AND DISCUSSION

A number of binary and polydisperse sets of mixtures were investigated for this study. Cases were considered where a significant degree of "separation" from the one-component case (see the Appendix) would be expected. Binary mixture simulations were carried out in which one of the three parameters (diameter ratio, σ_2/σ_1, mole fraction of the big spheres, x_1, and total volume fraction, η) was varied, while the remaining two were kept constant. An additional set was considered where σ_2/σ_1 and η changed linearly with x_1. Also the TH particle distribution was modeled for a range of $\sigma_{\rm min}/\sigma_{\rm max}$. Details of the sets of simulations carried out and the tags used for them are given in Table II. Note that, according to theory and by application of Eq. (2.25), the set of equimolar binary mixtures B1 and the set of polydisperse mixtures TH1 can be made equivalent. Similarly, the sets B5 and TH2 are theoretically equivalent.

The MD numerical values of $\bar{c}_2$, $\bar{c}_3$, $\beta\mu_1^{\rm ex}$, $\beta\mu_2^{\rm ex}$, Z, and $\beta a^{\rm ex}$ for the sets described in Table II are presented in Tables I–VIII of the supplementary material.

As for the different theoretical approaches summarized in Table I, we will discard the PY-v, PY-c, and PY-μ EoSs since they are known to be clearly inferior to the BMCSL or BCSK prescriptions.[12,30] Moreover, the differences (both absolute and relative) between the BMCSL and BCSK predictions for the coefficients $\bar{c}_2$ and $\bar{c}_3$ are smaller than the (already very small) differences in the one-component case (where $\bar{c}_2 \to c_2$ and $\bar{c}_3 \to c_3$). This can be explained by the fact that $\bar{c}_n^{\rm BMCSL} - \bar{c}_n^{\rm BCSK} = \lambda^n\left(c_n^{\rm BMCSL} - c_n^{\rm BCSK}\right)$ and $\lambda < 1$. Therefore, in what follows, we will mainly restrict ourselves to comparing the BMCSL EoS with our MD results.

The simulation and theoretical results for the binary systems B1–B4 and B6 are presented in Figs. 2–5 and 6, respectively. Figure 7 does the same for the continuous distribution TH1 and again for the binary mixture B1 [in the latter case by applying the mapping (2.26)], while Fig. 8 presents the results for systems B5 and TH2.

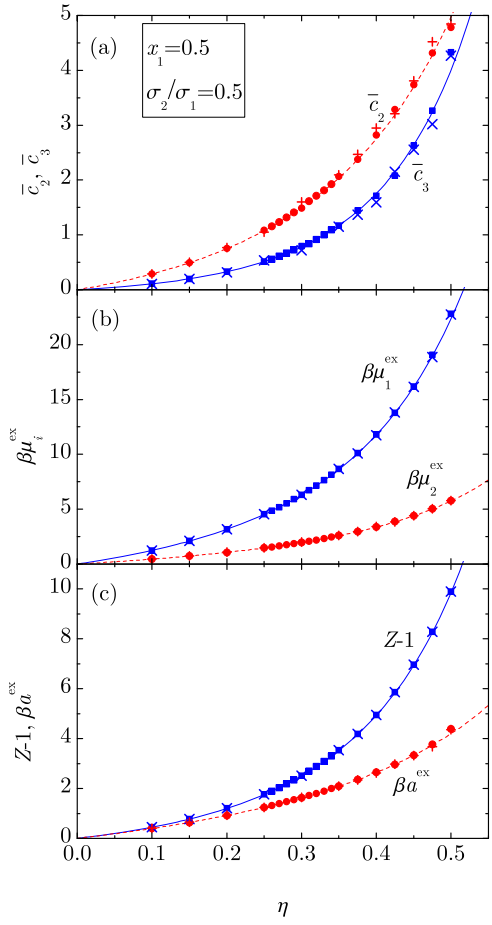

FIG. 5. Plot of (a) $\bar{c}_2$ and $\bar{c}_3$, (b) $\beta\mu_1^{\rm ex}$ and $\beta\mu_2^{\rm ex}$, and (c) $Z-1$ and $\beta a^{\rm ex}$ versus η for system B4. The symbols are our MD data (filled symbols: $N = 2048$, crosses: $N = 4000$) and the lines are the BMCSL predictions.

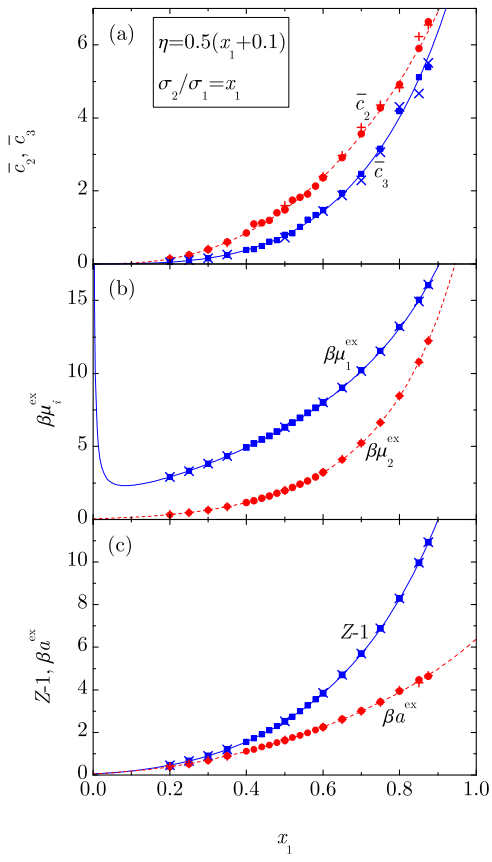

FIG. 6. Plot of (a) $\bar{c}_2$ and $\bar{c}_3$, (b) $\beta\mu_1^{\rm ex}$ and $\beta\mu_2^{\rm ex}$, and (c) $Z-1$ and $\beta a^{\rm ex}$ versus x_1 for system B6. The symbols are our MD data (filled symbols: $N = 2048$, crosses: $N = 4000$) and the lines are the BMCSL predictions.

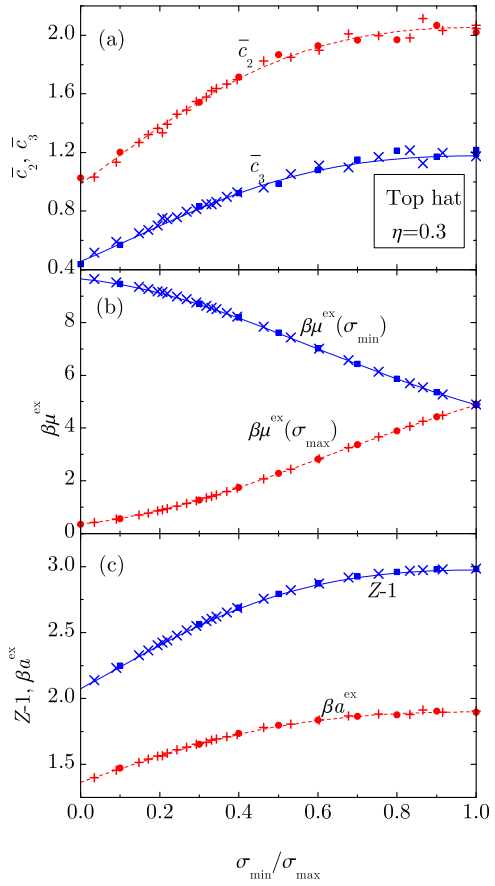

FIG. 7. Plots of (a) $\bar{c}_2$ and $\bar{c}_3$, (b) $\beta\mu^{ex}(\sigma_{min})$ and $\beta\mu^{ex}(\sigma_{max})$, and (c) $Z-1$ and βa^{ex} versus $\sigma_{min}/\sigma_{max}$ for system TH1 (squares and circles). The crosses represent results obtained from system B1 by application of the mapping (2.26). The symbols are our MD data ($N = 2048$) and the lines are the BMCSL predictions.

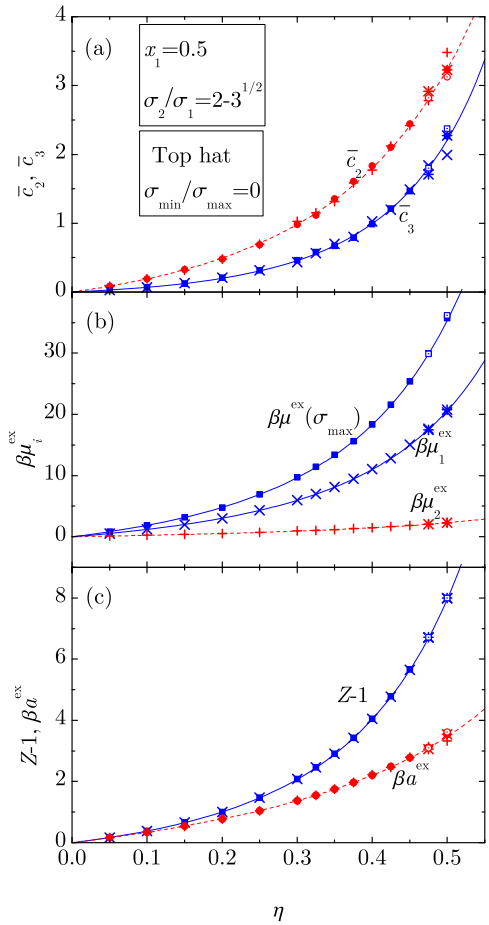

FIG. 8. Plots of (a) $\bar{c}_2$ and $\bar{c}_3$, (b) $\beta\mu_1^{ex}$, $\beta\mu_2^{ex}$, and $\beta\mu^{ex}(\sigma_{max})$, and (c) $Z-1$ and βa^{ex} versus η for systems B5 (crosses: $N = 2048$, stars: $N = 4000$) and TH2 (closed circles and squares: $N = 2048$, open circles and squares: $N = 4000$). The symbols are our MD data and the lines are the BMCSL predictions.

Even though the combined scope of these mixtures spans a wide spectrum of parameters, very good agreement of the BMCSL theory with the MD results is observed in all the cases. In particular, Figs. 7 and 8 confirm that systems as different as a binary mixture and a continuous size distribution can be practically indistinguishable from the thermodynamic point of view, provided they share the same values of λ and γ. Theory as well as simulation[31] strongly support that this mapping property extends to other continuous distributions different from the TH one.

Figures 2–8 show that, as expected, the fitting coefficients $\bar{c}_2$ and $\bar{c}_3$ present a certain degree of scatter. However, there is some "synergy" or compensation between these two quantities that takes place during the fitting process and reduces the level of scatter in the evaluation of the excess chemical potentials and the free energy via Eqs. (2.13) and (3.1), respectively. In any case, since the compressibility factor Z is measured directly in the simulations (rather than by a fitting algorithm), it is a more robust quantity. The excellent agreement found in Figs. 4–6, and 8 between the $N = 2048$ and $N = 4000$ sets of MD data gives us confidence in the lack of any statistically significant finite-size effects.

Despite the good behavior of the BMCSL theory observed in Figs. 2–8, a careful comparison shows that the theory generally underestimates the simulation values, especially in the case of the compressibility factor Z. The deviations $\Delta Z = Z - Z^{BMCSL}$ of the simulation data from the BMCSL predictions are plotted in Fig. 9, where also the deviations predicted by the BCSK EoS and the PY-μc EoS with $\alpha = 0.37$ [see Eq. (2.8)] are also included. We observe from Figs. 9(a), 9(b), 9(d), and 9(e) that at a packing fraction $\eta = 0.3$ one has $\Delta Z \approx 0.01$, practically with independence of the mixture composition. This property is very well accounted for by the PY-μc and, especially, BCSK theories. The same approximate value $\Delta Z \approx 0.01$ can be observed from Figs. 9(c) and 9(f) at $\eta = 0.3$ and from Fig. 9(f) at $x_1 = 0.5$ (which implies $\eta = 0.3$ in the set B6). As density increases in Figs. 9(c) and 9(f), ΔZ increases monotonically, reaching values close to $\Delta Z \approx 0.05$ at $\eta = 0.5$. This trend is well captured by the PY-μc EoS but not by the BCSK EoS. The latter presents a maximum deviation $\Delta Z = (\lambda^3/\gamma)\left(223 - 70\sqrt{10}\right)/81 \simeq 0.02\lambda^3/\gamma$ at $\eta = 2 - \sqrt{5/2} \simeq 0.42$ and then $\Delta Z = 0$ at $\eta = 0.5$. On the other hand, a similar non-monotonic behavior of ΔZ vs x_1 predicted by the BCSK EoS in Fig. 9(g) is actually confirmed by our simulations of the set B6, while the PY-μc EoS exhibits a monotonic behavior. Since increasing the mole fraction x_1 in the set B6 implies approaching a monodisperse system at higher densities, we can conclude that, at packing

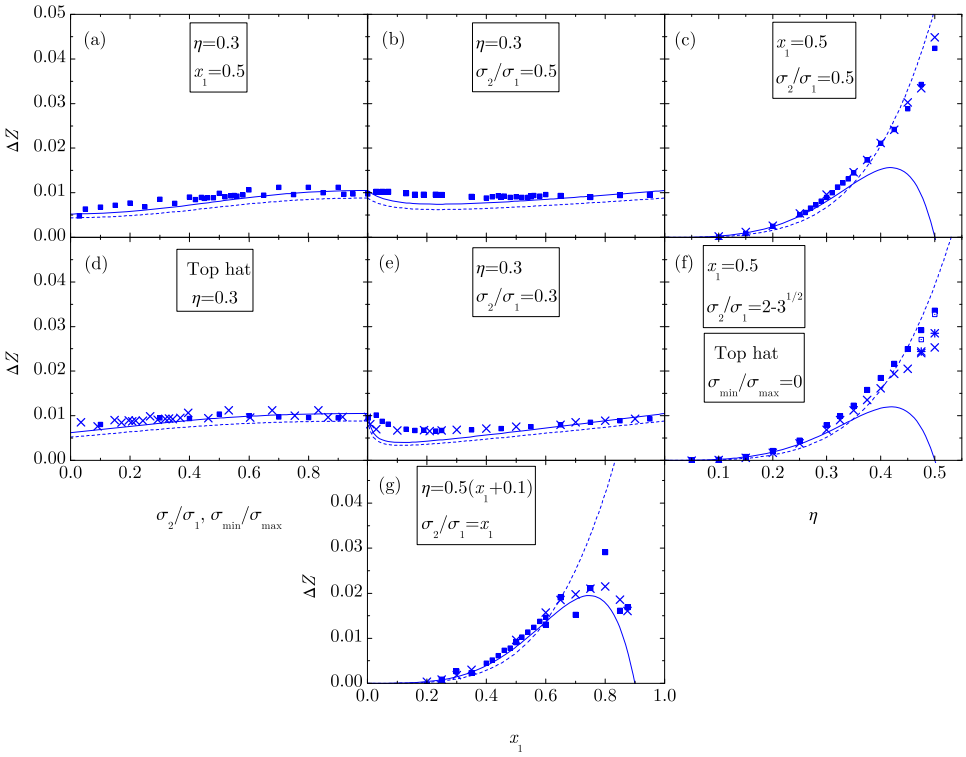

FIG. 9. Plots of the difference $\Delta Z = Z - Z^{\mathrm{BMCSL}}$ for systems (a) B1, (b) B2, (c) B4 (squares: $N = 2048$, crosses: $N = 4000$), (d) TH1 (squares), (e) B3 (squares: $N = 2048$, crosses: $N = 4000$), (f) B5 (crosses: $N = 2048$, stars: $N = 4000$) and TH2 (closed squares: $N = 2048$, open squares: $N = 4000$), and (g) B6 (squares: $N = 2048$, crosses: $N = 4000$). The symbols are our MD data and the solid and dashed lines represent $Z^{\mathrm{BCSK}} - Z^{\mathrm{BMCSL}}$ and $Z^{\mathrm{PY}-\mu c} - Z^{\mathrm{BMCSL}}$ (with $\alpha = 0.37$), respectively. The crosses in panel (d) represent results obtained from system B1 by application of the mapping (2.26).

fractions larger than about $\eta = 0.35$, the BCSK EoS is more accurate than the PY-μc EoS for nearly monodisperse systems ($\lambda^3/\gamma \lesssim 1$), but the opposite happens for mixtures where $1 - \lambda^3/\gamma$ is not small. For instance, $1 - \lambda^3/\gamma \simeq 0.23$ and 0.41 in Figs. 9(c) and 9(f), respectively, while $1 - \lambda^3/\gamma < 0.06$ for $x_1 > 0.7$ in Fig. 9(g). Finally, it is interesting to notice from Fig. 9(f) a very slight breaking down of the equivalence between the mixtures B5 and TH2 as density increases.

V. CONCLUSIONS

An extensive series of sets of MD simulations were carried out of the thermodynamic properties of binary and continuous size distribution HS mixtures. Relative particle diameters, mole fractions of the different components, and the total packing (volume) fraction were systematically varied. The Widom particle insertion method, employing the Labík and Smith technique,[11] was used to calculate the excess chemical potential of a test particle of variable diameter, σ_0. The simulation data were fitted to a third-order polynomial in σ_0, the first two coefficients of which are known exactly by theory. The compressibility factor, Z, was also independently obtained by a standard MD method. As a novel outcome, the excess free energy per particle was determined using a thermodynamic relation involving the compressibility factor and the two fitted coefficients.

The theories considered in this work share the same structure for the excess free energy and, hence, for the chemical potentials and the compressibility factor [see Eqs. (2.3), (2.10), and (2.13)]. These theories differ only in the density dependence of the coefficient $a_2(\eta)$ since the coefficients $Z_2(\eta)$, $c_2(\eta)$, and $c_3(\eta)$ are derived from $a_2(\eta)$ by thermodynamic relations [see Eqs. (2.11b) and (2.15)]. The most widely used theory in the literature is the BMCSL, which is an interpolation between the virial and compressibility routes in the PY approximation. Here we have also taken the BCSK (an *ad hoc* correction to the BMCSL EoS) and the PYμ-c theories. The latter is an interpolation between the chemical-potential and compressibility routes in the PY approximation and thus it has the same footing as the BMCSL theory.

Very good agreement between the simulation results with the predictions of the BMCSL analytic EoS is observed in all the cases. These simulations also confirm that systems as different as a binary mixture and a continuous size distribution can be hardly distinguishable in their thermodynamic quantities, provided they share the same values of the parameters λ and γ, which mark the extent of difference from the single component case.

A fine resolution examination of the MD generated quantities shows that the BMCSL theory typically underestimates the simulation values by a small amount, especially for the compressibility factor. These differences are generally captured well by the BCSK and PY-μc formulas (the latter with a mixing parameter $\alpha = 0.37$) in different regions of the system parameter space. When the packing fraction is larger than about $\eta = 0.35$, the PY-μc EoS is more accurate than the BCSK EoS, except for nearly monodisperse systems.

To conclude, we believe that the results reported here provide further evidence on the reliability of the BMCSL EoS over a wide spectrum of parameters characterizing a polydisperse HS fluid. On the other hand, the BCSK and PY-μc EoSs, while formally similar to the BMCSL EoS, succeed in improving the theoretical predictions. We expect that the MD simulation data obtained in this work can be useful to test other alternative theories proposed in the literature.

SUPPLEMENTARY MATERIAL

See supplementary material for tables containing the MD simulation results for the mixtures described in Table II.

ACKNOWLEDGMENTS

A.S. acknowledges the financial support of the Ministerio de Economía y Competitividad (Spain) through Grant No. FIS2016-76359-P, and of the Junta de Extremadura (Spain) through Grant No. GR18079, both partially financed by the "Fondo Europeo de Desarrollo Regional" funds. D.M.H. would like to thank Dr. T. Crane (Department of Physics, Royal Holloway, University of London, UK) for helpful software support.

APPENDIX: EXTREMAL PROPERTIES OF COMBINATIONS OF λ AND γ IN BINARY MIXTURES

In the framework of Eq. (2.3), the deviations of the compressibility factor of a mixture from that of the single component fluid (at a common value of the packing fraction η) are monitored by the (positive) differences $1-\lambda$ and $1-\lambda^3/\gamma$. In the case of a binary mixture characterized by the two parameters x_1 and $q=\sigma_2/\sigma_1 \le 1$, it can be checked that the maxima of $1-\lambda$ and $1-\lambda^3/\gamma$, at a fixed value of q, are

$$(1-\lambda)_{\max} = \frac{(1-\sqrt{q})^2(1+q)}{(1-\sqrt{q}+q)^2}, \tag{A1a}$$

$$\left(1-\frac{\lambda^3}{\gamma}\right)_{\max} = \frac{(1-q)^2(2+q)^2(1+2q)^2}{4(1+q+q^2)^3}. \tag{A1b}$$

Those maxima occur at

$$x_1 = \left(q^{-3/2}+1\right)^{-1}, \tag{A2a}$$

$$x_1 = \frac{q^2(2+q)}{(1+q)(1+q+q^2)}, \tag{A2b}$$

respectively.

In the case of the chemical potential, we see from Eqs. (2.13) and (2.14) that the deviations are now measured by the differences $1-\lambda^k$ (with $k=1, 2, 3$), $\gamma-\lambda^2$, $\gamma-\lambda^3$, and $\lambda(\gamma-\lambda^2)$. In the case of $1-\lambda^k$, the maxima are located at (A2a), but the analytical expressions of the locations for the other quantities are too cumbersome to be reproduced here.

Figure 10 shows the q-dependence of the mole fraction x_1 corresponding to the maxima of $1-\lambda^k$, $1-\lambda^3/\gamma$, $\gamma-\lambda^2$, $\gamma-\lambda^3$, and $\lambda(\gamma-\lambda^2)$. In all the cases, $x_1(q)$ decreases monotonically with decreasing q. In the limit $q\to 0$, while $x_1 \sim q^{3/2}$ and $x_1 \sim q^2$ in the cases of $1-\lambda^k$ and $1-\lambda^3/\gamma$, respectively, the asymptotic behavior is $x_1 \sim q^3$ in the cases of $\gamma-\lambda^2$, $\gamma-\lambda^3$, and $\lambda(\gamma-\lambda^2)$.

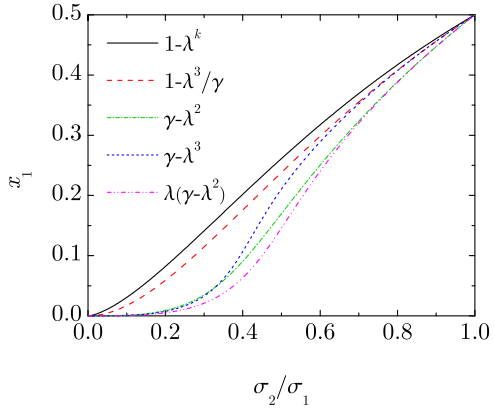

FIG. 10. Dependence on σ_2/σ_1 of the mole fraction corresponding to the maximum values of $1-\lambda^k$, $1-\lambda^3/\gamma$, $\gamma-\lambda^2$, $\gamma-\lambda^3$, and $\lambda(\gamma-\lambda^2)$.

[1] T. Boublík, "Hard-sphere equation of state," J. Chem. Phys. **53**, 471–472 (1970).
[2] G. A. Mansoori, N. F. Carnahan, K. E. Starling, and T. W. Leland, Jr., "Equilibrium thermodynamic properties of the mixture of hard spheres," J. Chem. Phys. **54**, 1523–1525 (1971).
[3] D. H. L. Yau, K.-Y. Chan, and D. Henderson, "A further test of the Boublik *et al*. equations for binary hard sphere mixtures," Mol. Phys. **88**, 1237–1248 (1996).
[4] M. Barošová, A. Malijevský, S. Labík, and W. R. Smith, "Computer simulation of the chemical potentials of binary hard-sphere mixtures," Mol. Phys. **87**, 423–439 (1996).
[5] A. Liu, "Calculation of chemical potentials of mixtures from computer simulations," Mol. Phys. **89**, 1651–1658 (1996).
[6] L. Lue and L. V. Woodcock, "Depletion effects and gelation in a binary hard-sphere fluid," Mol. Phys. **96**, 1435–1443 (1999).
[7] M. Tokuyama and Y. Terada, "Slow dynamics and re-entrant melting in a polydisperse hard-sphere fluid," J. Phys. Chem. B **109**, 21357–21363 (2005).
[8] C. Barrio and J. R. Solana, "Binary mixtures of additive hard spheres. Simulations and theories," in *Theory and Simulation of Hard-Sphere Fluids and Related Systems*, Lecture Notes in Physics, edited by A. Mulero (Springer-Verlag, Berlin, 2008), Vol. 753, pp. 133–182.
[9] G. Odriozola and L. Berthier, "Equilibrium equation of state of a hard sphere binary mixture at very large densities using replica exchange Monte Carlo simulations," J. Chem. Phys. **134**, 054504 (2011).
[10] B. Widom, "Some topics in the theory of fluids," J. Chem. Phys. **39**, 2808–2812 (1963).
[11] S. Labík and W. R. Smith, "Scaled particle theory and the efficient calculation of the chemical potential of hard spheres in the NVT ensemble," Mol. Simul. **12**, 23–31 (1994).
[12] D. M. Heyes and A. Santos, "Chemical potential of a test hard sphere of variable size in a hard-sphere fluid," J. Chem. Phys. **145**, 214504 (2016).
[13] V. Baranau and U. Tallarek, "Chemical potential and entropy in monodisperse and polydisperse hard-sphere fluids using Widom's particle insertion method and a pore size distribution-based insertion probability," J. Chem. Phys. **144**, 214503 (2016).
[14] D. M. Heyes, "Chemical potential, partial enthalpy and partial volume of mixtures by NPT molecular dynamics," Chem. Phys. **159**, 149–167 (1992).
[15] C. Perego, F. Giberti, and M. Parrinello, "Chemical potential calculations in dense liquids using metadynamics," Eur. Phys. J. Spec. Top. **225**, 1621–1628 (2016).
[16] O. Valsson, P. Tiwary, and M. Parrinello, "Enhancing important fluctuations: Rare events and metadynamics from a conceptual viewpoint," Annu. Rev. Phys. Chem. **67**, 159–184 (2016).
[17] A. Santos, S. B. Yuste, and M. López de Haro, "Equation of state of a multicomponent d-dimensional hard-sphere fluid," Mol. Phys. **96**, 1–5 (1999).
[18] A. Santos, S. B. Yuste, and M. López de Haro, "Virial coefficients and equations of state for mixtures of hard discs, hard spheres, and hard hyperspheres," Mol. Phys. **99**, 1959–1972 (2001).
[19] A. Santos, S. B. Yuste, and M. López de Haro, "Contact values of the radial distribution functions of additive hard-sphere mixtures in d dimensions: A new proposal," J. Chem. Phys. **117**, 5785–5793 (2002).
[20] A. Santos, S. B. Yuste, and M. López de Haro, "Contact values of the particle-particle and wall-particle correlation functions in a hard-sphere polydisperse fluid," J. Chem. Phys. **123**, 234512 (2005).
[21] H. Hansen-Goos and R. Roth, "A new generalization of the Carnahan-Starling equation of state to additive mixtures of hard spheres," J. Chem. Phys. **124**, 154506 (2006).
[22] P. Paricaud, "Extension of the BMCSL equation of state for hard spheres to the metastable disordered region: Application to the SAFT approach," J. Chem. Phys. **143** 044507 (2015).

[23] A. Mulero, C. A. Galán, M. I. Parra, and F. Cuadros, "Equations of state for hard spheres and hard disks," in *Theory and Simulation of Hard-Sphere Fluids and Related Systems*, Lecture Notes in Physics, edited by A. Mulero (Springer-Verlag, Berlin, 2008), Vol. 753, pp. 37–109.
[24] J. L. Lebowitz and D. Zomick, "Mixtures of hard spheres with nonadditive diameters: Some exact results and solution of PY equation," J. Chem. Phys. **54**, 3335–3346 (1971).
[25] J. W. Perram and E. R. Smith, "A model for the examination of phase behaviour in multicomponent systems," Chem. Phys. Lett. **35**, 138–140 (1975).
[26] B. Barboy, "Solution of the compressibility equation of the adhesive hard-sphere model for mixtures," Chem. Phys. **11**, 357–371 (1975).
[27] J. K. Percus and G. J. Yevick, "Analysis of classical statistical mechanics by means of collective coordinates," Phys. Rev. **110**, 1–13 (1958).
[28] A. Santos, *A Concise Course on the Theory of Classical Liquids. Basics and Selected Topics*, Lecture Notes in Physics (Springer, New York, 2016), Vol. 923.
[29] A. Santos, "Chemical-potential route: A hidden Percus–Yevick equation of state for hard spheres," Phys. Rev. Lett. **109**, 120601 (2012).
[30] A. Santos and R. D. Rohrmann, "Chemical-potential route for multicomponent fluids," Phys. Rev. E **87**, 052138 (2013).
[31] V. Ogarko and S. Luding, "Equation of state and jamming density for equivalent bi- and polydisperse, smooth, hard sphere systems," J. Chem. Phys. **136**, 124508 (2012).
[32] H. Reiss, H. L. Frisch, and J. L. Lebowitz, "Statistical mechanics of rigid spheres," J. Chem. Phys. **31**, 369–380 (1959).
[33] J. L. Lebowitz, E. Helfand, and E. Praestgaard, "Scaled particle theory of fluid mixtures," J. Chem. Phys. **43**, 774–779 (1965).
[34] M. Mandell and H. Reiss, "Scaled particle theory: Solution to the complete set of scaled particle theory conditions: Applications to surface structure and dilute mixtures," J. Stat. Phys. **13**, 113–128 (1975).
[35] Y. Rosenfeld, "Scaled field particle theory of the structure and thermodynamics of isotropic hard particle fluids," J. Chem. Phys. **89**, 4272–4287 (1988).
[36] M. Heying and D. Corti, "Scaled particle theory revisited: New conditions and improved predictions of the properties of the hard sphere fluid," J. Phys. Chem. B **108**, 19756–19768 (2004).
[37] M. López de Haro, S. B. Yuste, and A. Santos, "Alternative approaches to the equilibrium properties of hard-sphere liquids," in *Theory and Simulation of Hard-Sphere Fluids and Related Systems*, Lecture Notes in Physics, edited by A. Mulero (Springer, Berlin, 2008), Vol. 753, pp. 183–245.
[38] A. Santos, S. B. Yuste, and M. López de Haro, "Communication: Inferring the equation of state of a metastable hard-sphere fluid from the equation of state of a hard-sphere mixture at high densities," J. Chem. Phys. **135**, 181102 (2011).
[39] A. Santos, "Class of consistent fundamental-measure free energies for hard-sphere mixtures," Phys. Rev. E **86**, 040102(R) (2012).
[40] A. Santos, S. B. Yuste, M. López de Haro, G. Odriozola, and V. Ogarko, "Simple effective rule to estimate the jamming packing fraction of polydisperse hard spheres," Phys. Rev. E **89**, 040302(R) (2014).
[41] N. F. Carnahan and K. E. Starling, "Equation of state for nonattracting rigid spheres," J. Chem. Phys. **51**, 635–636 (1969).
[42] T. Boublík and I. Nezbeda, "P-V-T behaviour of hard body fluids. Theory and experiment," Collect. Czech. Chem. Commun. **51**, 2301–2432 (1986).
[43] T. Boublík, "Equations of state of hard body fluids," Mol. Phys. **59**, 371–380 (1986).
[44] H. Reiss, H. L. Frisch, E. Helfand, and J. L. Lebowitz, "Aspects of the statistical thermodynamics of real fluids," J. Chem. Phys. **32**, 119–124 (1960).
[45] R. Roth, R. Evans, A. Lang, and G. Kahl, "Fundamental measure theory for hard-sphere mixtures revisited: The white bear version," J. Phys.: Condens. Matter **14**, 12063–12078 (2002).
[46] B. J. Alder, "Studies in molecular dynamics. III. A mixture of hard spheres," J. Chem. Phys. **40**, 2724–2730 (1964).
[47] A. Rotenberg, "Monte Carlo equation of state for hard spheres in an attractive square well," J. Chem. Phys. **43**, 1198–1201 (1965).
[48] M. N. Bannermana and L. Lue, "Transport properties of highly asymmetric hard-sphere mixtures," J. Chem. Phys. **130**, 164507 (2009).
[49] T. Biben and J.-P. Hansen, "Phase separation of asymmetric binary hard-sphere fluids," Phys. Rev. Lett. **66**, 2215–2218 (1991).
[50] M. Dijkstra, R. van Roij, and R. Evans, "Phase diagram of highly asymmetric binary hard-sphere mixtures," Phys. Rev. E **59**, 5744–5771 (1999).
[51] D. A. Kofke and P. G. Bolhuis, "Freezing of polydisperse hard spheres," Phys. Rev. E **59**, 618–622 (1999).